Ships and Offshore Structures
Publication details, including instructions for authors and subscription information:
http://www.tandfonline.com/loi/tsos20

Interactive buckling tests on steel cones subjected to axial compression and external pressure - a comparison of experimental data and design codes

O. Ifayefunmi[a]
[a] Faculty of Engineering Technology, Universiti Teknikal Malaysia Melaka, Melaka, Malaysia
Published online: 05 Dec 2013.

To cite this article: O. Ifayefunmi , Ships and Offshore Structures (2013): Interactive buckling tests on steel cones subjected to axial compression and external pressure - a comparison of experimental data and design codes, Ships and Offshore Structures, DOI: 10.1080/17445302.2013.862987

To link to this article: http://dx.doi.org/10.1080/17445302.2013.862987

Ships and Offshore Structures, 2013
http://dx.doi.org/10.1080/17445302.2013.862987

Interactive buckling tests on steel cones subjected to axial compression and external pressure – a comparison of experimental data and design codes

O. Ifayefunmi*

Faculty of Engineering Technology, Universiti Teknikal Malaysia Melaka, Melaka, Malaysia

(*Received 4 March 2013; accepted 2 November 2013*)

The plastic buckling of thick steel conical shells subjected to combined action of axial compression and external pressure is of considerable interest in the offshore and the nuclear industries. However, design information on this subject area is limited. At present, only the ASME B&PV code case 2286-2 provides design information for cones subjected to axial and hoop compressions acting simultaneously. This design rule has not been validated both experimentally and numerically, especially in the elastic–plastic region. Past results on interactive buckling tests carried out at the University of Liverpool, Liverpool, UK on 13 computer numerically controlled (CNC)-machined cones having $r_2/r_1 = 2.02$, $r_2/t = 34.3$, $h/r_2 = 1.01$, and $\beta = 26.56^\circ$ were compared with predictions of design loads obtained from ASME code case 2286-2. This was done in order to check the applicability of this design rule and suggest a safe operating region. The paper consider the general procedure adopted by the ASME case code 2286-2 to predict the interactive buckling curve and identifies some discrepancies in the predictions. It further suggests region of safe operational design level. Combined stability plots for the master cone and equivalent cylinder have also been derived. Results of this study show that 'the equivalent cylinders' do not represent a safe design substitute for a relatively thick cone under combined loading.

Keywords: interactive buckling; axial compression; external pressure; combined loading; elastic–plastic; ASME design codes; equivalent cylinder; mild steel cones

1. Introduction

Thick conical shells subjected to simultaneous action of axial compression and external pressure are a major structural component used in the nuclear industry (for flue gas desulphurisation vessel) and offshore industry (for the legs of offshore drilling rig). In these applications, the radius-to-thickness ratio is low and the buckling is usually within the elastic–plastic range. However, it is surprising that the amount of experimental data for this plastic interactive buckling problem is so limited. Therefore, the design information available for this kind of shell buckling problem cannot be relied on.

Results of recent test data on elastic–plastic buckling of cones subjected to axial compression and external pressure carried out in Liverpool are reported in Ifayefunmi (2011), Blachut (2012), Blachut and Ifayefunmi (2012), and Ifayefunmi and Blachut (2012). Tests were on relatively thick steel cones. Blachut and Ifayefunmi (2012), Ifayefunmi and Blachut (2012), and Ifayefunmi (2011) were devoted to cones with radius-to-thickness ratio $r_2/t = 34.3$ and semi-vertex angle $\beta = 26.56^\circ$, while Blachut (2012) covers cones with larger radius-to-thickness ratio $r_2/t = 50$ and semi-vertex angle $\beta = 14^\circ$.

Motivation for the current paper originates from the fact that the state of knowledge of the available design codes on buckling of unstiffened steel conical shells subjected to combined loading, i.e., axial compression and external pressure acting simultaneously, is limited. At present, only ASME B&PV code case 2286-2 (ASME 2008) provides design information for cones subjected to axial and hoop compressions acting simultaneously. Blachut (2012), Ifayefunmi and Blachut (2012), and Ifayefunmi (2011) present recent investigations into the predictions of interactive plot given by ASME code case 2286-2 for failure load of cones subjected to combined axial compression and external pressure within the plastic region.

From Blachut (2012), Ifayefunmi and Blachut (2012), and Ifayefunmi (2011), it can be seen that a large portion of the interactive axial compression and external pressure curve for cones is on the unsafe side of the first yield envelope but on the safe side of the collapse envelope. However, when considering the buckling behaviour of relatively thick cones which usually fails in the elastic–plastic region, this is a major design issue. Since under low-level cycling, it is immaterial what happened within the elastic domain, but for cones in the elastic–plastic domain, each cycle induces

* Email: olawale@utem.edu.my

a permanent deformation on the cone, thereby reducing the cone's load-carrying capacity. Then, it is important to establish the range of applicability of these design codes.

Traditionally, the design of cones has been based on the equivalent cylinder approach. The conical shell was treated as a cylindrical shell with an equivalent geometry for the purpose of obtaining the buckling strength. Several analytical and experimental research works have been carried out to correlate buckling of conical shells with buckling of the equivalent cylindrical shells. Cases of axial compression only, or external pressure only, were attempted in Seide (1956), Seide (1959), Lackman and Penzien (1960), Singer (1962), Singer (1963), Singer and Eckstein (1963), Singer (1965), Weingarten et al. (1965), Singer (1966), Tani (1971), Samuelson and Eggwertz (1992), Yeh et al. (1995), Singer et al. (2002), and Barkey et al. (2008). But there has not been any work for equivalent cylinder approach related to combined stability reported, except for recent work published by Blachut (2010, 2011). Hence, there is a need to examine the influence of different equivalent cylinder radii on the domain of combined stability for equivalent cylinder.

The current contribution considers the general procedure adopted by ASME case code 2286-2, to predict the plastic interactive buckling curve for steel cones subjected to axial compression and external pressure. Test data reported by Ifayefunmi and Blachut (2012) were compared with prediction of design load obtained from ASME code case 2286-2 for thick mild steel cone with radius-to-thickness ratio $r_2/t = 34.3$. The paper then suggests region of safe operational design level for this specific problem. Also, the paper further examines the influence of different equivalent cylinder radii on the domain of combined stability plot of equivalent cylinder for thick mild steel cone with radius-to-thickness ratio $r_2/t = 34.3$.

2. Background – finite element modelling of truncated cone

A truncated cone with small and big radii r_1 and r_2, respectively, uniform wall thickness t, height of the shell h, cone slant length L, and the cone angle β is considered. Here, it was assumed that the cone is subjected to axial compression and external pressure acting simultaneously, as shown in Figure 1a.

The edge support at both the bottom and the top ends of the cone is illustrated in Figure 1a, i.e., the cone is clamped at the big radius end and allowed to move axially at the small radius end.

Some preliminary numerical calculations have been carried out in Liverpool to illustrate typical buckling behaviour of conical shells subjected to axial compression and external pressure, details can be found in Ifayefunmi (2011). The numerical results are obtained using ABAQUS finite element (FE) code (Hibbitt et al. 2006). The ABAQUS analysis was both axisymmetric and two-dimensional. Convergence studies indicated that 70 SAX2 elements and 142 axial by

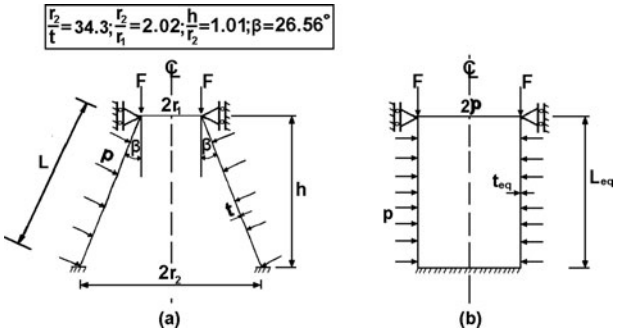

Figure 1. Geometry of (a) master cone and (b) equivalent cylinder with equivalent radius ρ subjected to combined action of axial compression and external pressure acting simultaneously.

40 hoop S8R elements are sufficient for the analysis. The material of the cone was modelled as elastic perfectly plastic. It is assumed that cones are made from mild steel with the following material properties: Young's modulus $E = 210.49$ GPa, yield stress $\sigma_{yp} = 230.6$ MPa, and Poisson's ratio $\nu = 0.281$. The range of (radius-to-thickness) ratio investigated was $34.3 \leq r_2/t \leq 250$. Typical results obtained from numerical calculations are given in the following subsection.

2.1. Numerical predictions – cones subjected to axial compression and external pressure

Numerical predictions showing comparisons of combined stability plot for cone with different r_2/t values (i.e., $34.3 \leq r_2/t \leq 250$) subjected to axial compression and external pressure are presented in Figure 2. For different r_2/t ratio, 25 different points (simulations) were used to define the interactive plot. From Figure 2, two distinct regions can be

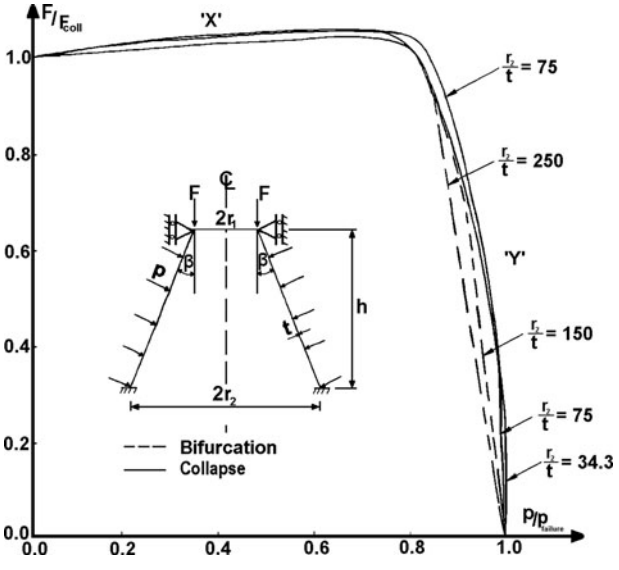

Figure 2. Domain of combined stability plot for different r_2/t values.

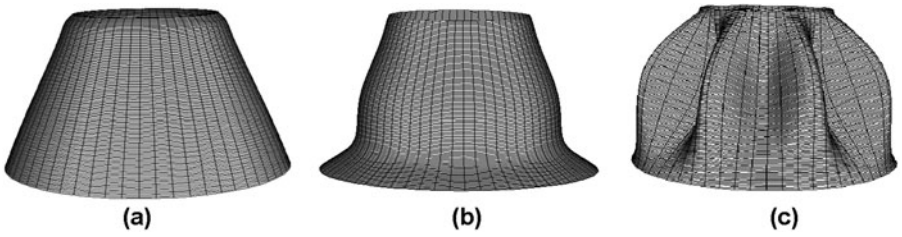

Figure 3. View of cones with axisymmetric collapse under axial compression (a), axisymmetric collapse under external pressure (b), and asymmetric bifurcation under external pressure (c).

identified, i.e., 'X' – force dominant region and 'Y' – pressure dominant region. In the region 'X', the cone failure is controlled by the axial force, i.e., constant pressure of known magnitude is applied to the cone, and at this constant pressure search for the axial load that will cause the cone to fail. In region 'Y', the cone failure is dominated by external pressure, i.e., constant force of known magnitude is applied to the cone, and at this constant force search for the pressure at which the cone will fail. Figure 2 reveals that all the interactive plots show similar trend except that for $r_2/t < 150$, where the failure loads are always limited by axisymmetric collapse. Typical views of axisymmetric collapse cones under axial compression and external pressure are shown in Figure 3a and 3b, respectively. For cones with $r_2/t > 150$, there are two mechanisms of failure, i.e., asymmetric bifurcation and axisymmetric collapse. Once the axial load approaches the collapse magnitude, the resistance to external pressure rapidly diminishes, and the mode of failure switches over from asymmetric bifurcation to axisymmetric collapse. Figure 3c depicts a view of asymmetric bifurcation of cone subjected to external pressure. Also, it can be observed from Figure 2 that increasing the radius-to-thickness ratio leads to the interactive plots becoming smaller.

However, when considering the buckling behaviour of relatively thick cones which usually fails in the elastic–plastic region, it is expected that plastic straining will occur before the cone's failure. In cases like this, the loading path can affect the magnitude and mechanism of cone's failure. Therefore, it was decided to investigate the regions of purely elastic behaviour and region where plastic straining occurs. Figure 4 depicts the corresponding domain of interactive plot for cone with $r_2/t = 75$ and 250, highlighting the regions of purely elastic behaviour and region where plastic straining occurs. Details of other radius-to-thickness ratio (r_2/t) can be found in Ifayefunmi (2011).

2.2. *Numerical predictions – equivalent cylinder subjected to axial compression and external pressure*

This subsection examines the influence of different equivalent cylinder radii on the domain of combined stability plot of equivalent cylinder for thick mild steel cone with

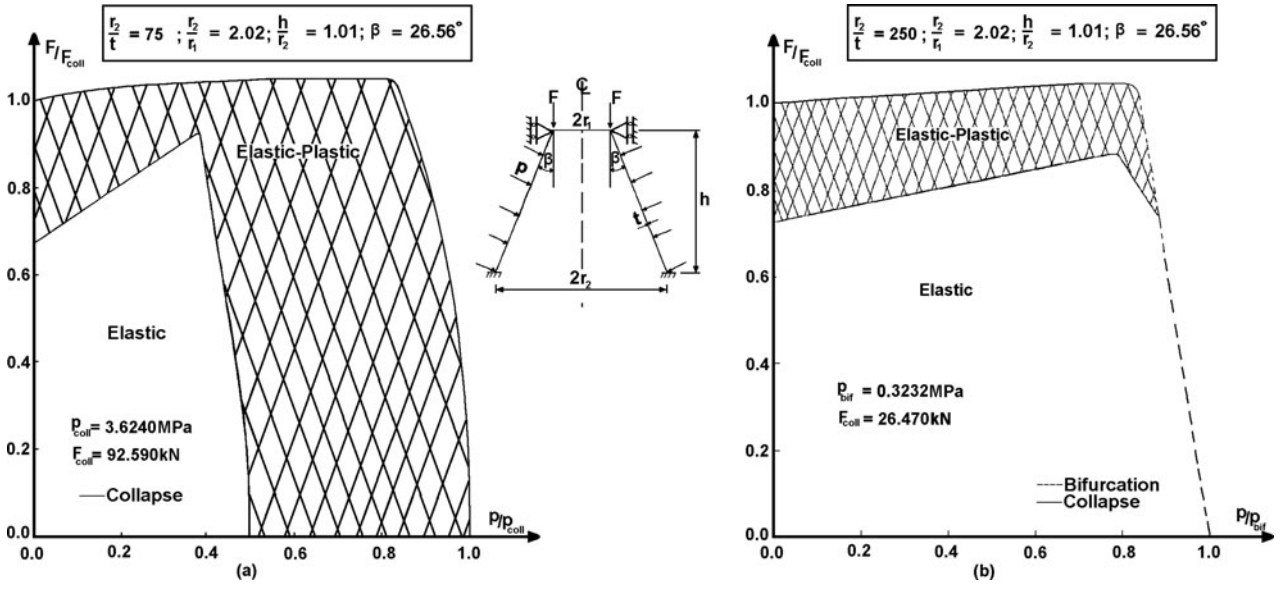

Figure 4. Domain of combined stability plot for $r_2/t = 75$ (a), and for $r_2/t = 250$ (b).

radius-to-thickness ratio $r_2/t = 34.3$. Geometry and boundary conditions of analysed shells are the same as in experiments (see Ifayefunmi 2011 for details).

It is customary to link the design of cones to the equivalent cylinder approach. Past studies show that there are discrepancies on the choice of the equivalent cylinder radius. Therefore, several possibilities have been suggested by DIN 18 800 (1990), DnV CN 30.1 (1992), Samuelson and Eggwertz (1992), Schmidt and Krysik (1994), and ECCS TWG 8.4 (2008)).

Consider a master cone having geometry described in Section 2 with radius-to-thickness ratio $r_2/t = 34.3$. This master cone has an equivalent cylindrical shell sketched in Figure 1b, with equivalent radius ρ, equivalent wall thickness t_{eq}, and the equivalent length given by L_{eq}. Assume that the cylinder is subjected to combined action of axial compression F and external pressure p acting simultaneously. Let the equivalent cylinder have the same boundary conditions at the bottom and top ends as the cone has, as shown in Figure 1b.

The FE calculations were carried out for equivalent cylinders having the radius given by Schmidt and Krysik (1994) (Case 1), DnV CN 30.1 (1992) (Case 2), and Samuelson and Eggwertz (1992) (Case 3). Results for other possibilities such as DIN 18 800 (1990) and ECCS TWG 8.4 (2008) can be found in Blachut (2011).

$$\text{Case 1:} \quad \rho = \frac{r_1 + r_2}{2} = 74.0 \text{ mm} \tag{1}$$

$$\text{Case 2:} \quad \rho = \frac{r_1 + r_2}{2\cos\beta} = 82.73 \text{ mm} \tag{2}$$

$$\text{Case 3:} \quad \rho(r_1 + 2\sqrt{r_1 t \sin\beta}) = \frac{r_1 + 2\sqrt{r_1 t \sin\beta}}{\cos\beta} = 66.68 \text{ mm} \tag{3}$$

All these cylinders had constant wall thickness of 2.89 mm, and they were derived from $r_1 = 49$ mm and $r_2 = 99$ mm (master cone). The length of all equivalent cylinders is the same and it is equal to the slant length of the master cone. Also, equivalent cylinder was assumed to be made from mild steel with the following material properties: Young's modulus $E = 210.49$ GPa, the yield point $\sigma_{yp} = 230.6$ MPa, and Poisson's ratio $\nu = 0.281$, same as the master cone which they represent. In a similar manner to the master cone, 25 different points (simulations) were used to define the interactive plot for different cases of equivalent cylinder.

Figure 5 presents comparisons of combined stability envelopes for equivalent cylinder with different equivalent cylinder radii. It can be seen that all the interactive plots show a similar trend (i.e., they are all convex). The load-carrying capacity is always limited by axisymmetric collapse. Also, it can be noticed from Figure 5 that decreasing the equivalent cylinder radius leads to the interactive plots becoming wider.

It must be noted that the axes in Figure 5 are normalised by the respective collapse load (force and pressure) for each cases considered. Hence, for better comparison, it was decided to present the combined stability plot for the master cone and the equivalent cylinders, normalised by the collapse load (force and pressure) of the master cone.

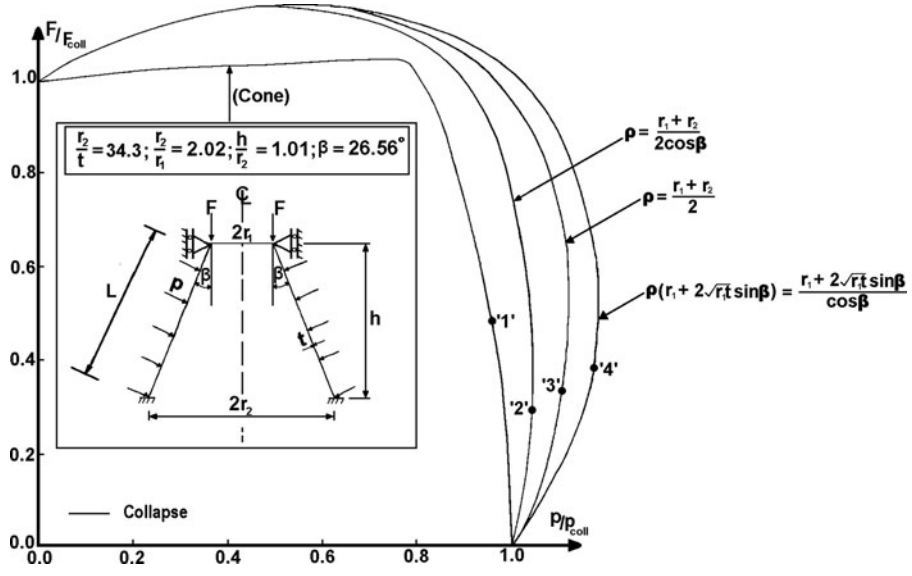

Figure 5. Domain of combined stability plot for master cone with $r_2/t = 34.3$, and for equivalent cylinder of three different equivalent radii. Note: The axes are normalised by the respective collapse load (force and pressure) for each cases considered. See Table 1 for absolute values corresponding to points '1', '2', '3', and '4'.

Table 1. Comparison of failure load of master cone with those of equivalent cylinders. Points '1', '2', '3', and '4' are indicated on Figures 5 and 6. The underlined value is usually used in equivalent design approach.

		Load-carrying capacity (kN, MPa)		
		(F, p)	(F, p)	(F, p)
Master cone		(0.0, 8.498)	(210.0, 0.0)	(100.0, 8.318)'1'
Equivalent cylinders	Case 1	(0.0, 9.151)	(317.2, 0.0)	(100.0, 10.12)'3'
	Case 2	(0.0, <u>8.640</u>)	(354.0, 0.0)	(100.0, 9.026)'2'
	Case 3	(0.0, 9.628)	(286.4, 0.0)	(100.0, 11.28)'4'

The resulting graph is shown in Figure 6. Table 1 presents the comparison of collapse load of master cone with those of equivalent cylinder subjected to combined loading. For each case, the magnitudes of the following situations are given:

(1) Collapse pressure under zero axial compression (column 3).

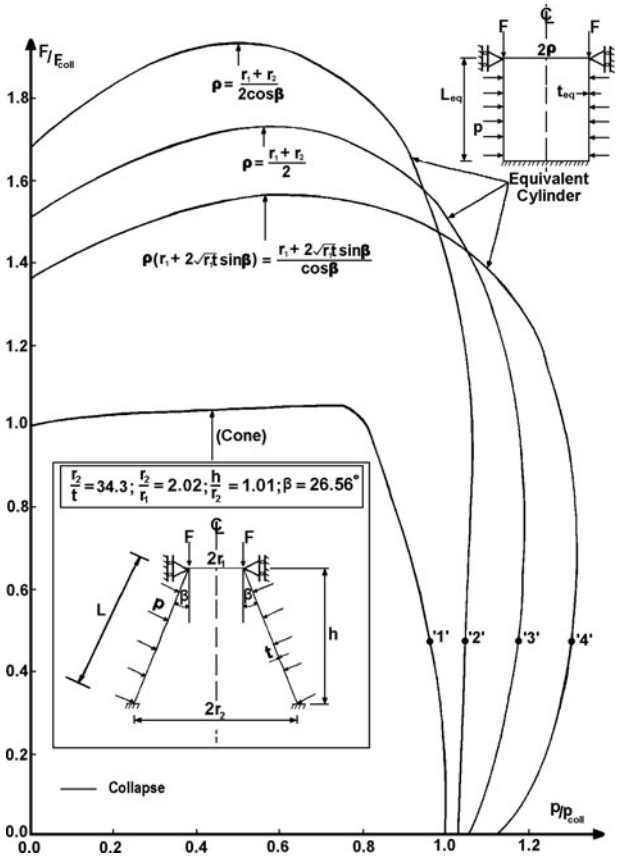

Figure 6. Domain of combined stability plot for master cone with $r_2/t = 34.3$, and for equivalent cylinder of three different equivalent radii. Note: The axes are normalised by the collapse load (force and pressure) of the master cone. See Table 1 for absolute values corresponding to points '1', '2', '3', and '4'.

(2) Collapse force for zero pressure (column 4).
(3) Collapse pressure for a fixed axial compression of $F = 100$ kN (column 5).

It is clear from Table 1 that all, except one case, configurations of equivalent cylinders have higher values of collapse load than the master cone which they meant to represent. The three above cases (i.e., Case 1, Case 2, and Case 3) do not cover the equivalent cylinder radius used by design codes for axial compression. Hence 'the equivalent cylinders' do not represent a safe design substitute for a relatively thick cone under combined loading.

3. Experimentation – general

Tests on 13 conical specimens (C1–C13), CNC machined with integral top and bottom flanges from 252 mm diameter steel billet, were conducted. The specimens were made from mild steel. To establish the buckling behaviour of cones along the combined stability plot, all cones were nominally identical with nominal dimensions given by $r_2/r_1 = 2.02$, $r_2/t = 33.0$, $h/r_2 = 1.01$, $\beta = 26.56^\circ$, and the wall thickness $t = 3$ mm.

Prior to tests, pretest measurements were carried out on all the cone specimens. Cones were marked and measured at 16 points around the circumference at 22.5° intervals and at 12 different equidistant points along the cone slant. Table 2 gives the summary of measured wall thickness together with other measured quantities. Details about the measurement process, testing procedure, and collapse test results can be found in (Ifayefunmi (2011) and Ifayefunmi and Blachut (2012)).

3.1. *Collapse test*

Figure 7a illustrates the sequence in which load was applied to all tested models. This loading sequence is the same as those used for numerical calculations. Prior to testing, cones were covered with top and bottom plates which help to create desired boundary conditions, i.e., fully clamped.

Table 2. Measured data for all tested cones. Note: $\Delta t_{ave} \equiv$ standard deviations and $r \equiv$ mid-surface radius.

	t_{min}	t_{max}	t_{ave}	Δt_{ave}	$\overline{r_2}$				
	(mm)					$\overline{r_2}/\overline{r_1}$	$\overline{r_2}/t_{ave}$	$h_{ave}/\overline{r_2}$	β_{ave} (deg)
C1	2.86	2.93	2.89	0.014	100.62	1.992	34.82	0.993	26.37
C2	2.88	2.92	2.90	0.009	100.53	1.989	34.68	1.002	26.37
C3	2.80	2.84	2.82	0.011	100.58	1.988	35.67	0.995	26.36
C4	2.89	2.92	2.90	0.008	100.57	1.990	34.68	0.995	26.53
C5	2.88	2.96	2.92	0.018	100.62	1.989	34.46	0.995	26.42
C6	2.94	3.01	2.97	0.014	100.66	1.989	33.89	0.994	26.47
C7	2.88	2.93	2.90	0.012	100.57	1.989	34.68	0.995	26.51
C8	2.87	2.95	2.91	0.020	100.60	1.992	34.57	0.997	26.48
C9	2.73	2.89	2.82	0.041	100.52	1.994	35.65	1.002	26.42
C10	2.76	2.87	2.81	0.025	100.30	1.986	35.69	0.997	26.47
C11	2.87	2.97	2.92	0.019	100.59	1.988	34.45	0.994	26.56
C12	2.82	2.91	2.87	0.024	100.39	1.987	34.98	0.996	26.51
C13	3.20	3.26	3.23	0.015	100.78	1.985	31.20	0.991	26.53

Two cones (C3 and C4) were subjected to axial compression, with further two (C11 and C13) subjected to lateral external pressure. Cones (C1 and C2) were tested under hydrostatic external pressure. The remaining seven cones (C5–C10 and C12) were subjected to combined action of axial compression and external pressure.

Cones C3 and C4 were placed between platens of compression machine. Whilst, the remaining cones were immersed into the experimental rig which has a diameter of 350 mm and total length of 1000 mm with a maximum working pressure of 40.0 MPa. The failure loads for all tested cones are presented in column 3 of Table 3 and their corresponding collapse shape is shown in Figure 7b. There was no difficulty in identifying the failure load of the cones.

4. Guidance from ASME B&PV code case 2286-2

From the practical point of view, the design of cones for the case of combined loading, i.e., axial compression and external pressure, is only covered by ASME code case 2286-2. This formulation is only applicable for cones with slenderness factor $\lambda_c \leq 0.15$. Five major steps are required to achieve this. They are listed below.

(1) Establish the value of the slenderness factor λ_c.

$$\lambda_c = \frac{KL_u}{\pi r}\sqrt{\frac{\sigma_{xc}\mathrm{FS}}{E}} \tag{4}$$

(2) Determine the allowable local compressive membrane stress due to axial compression σ_{xc}. σ_{xc} is

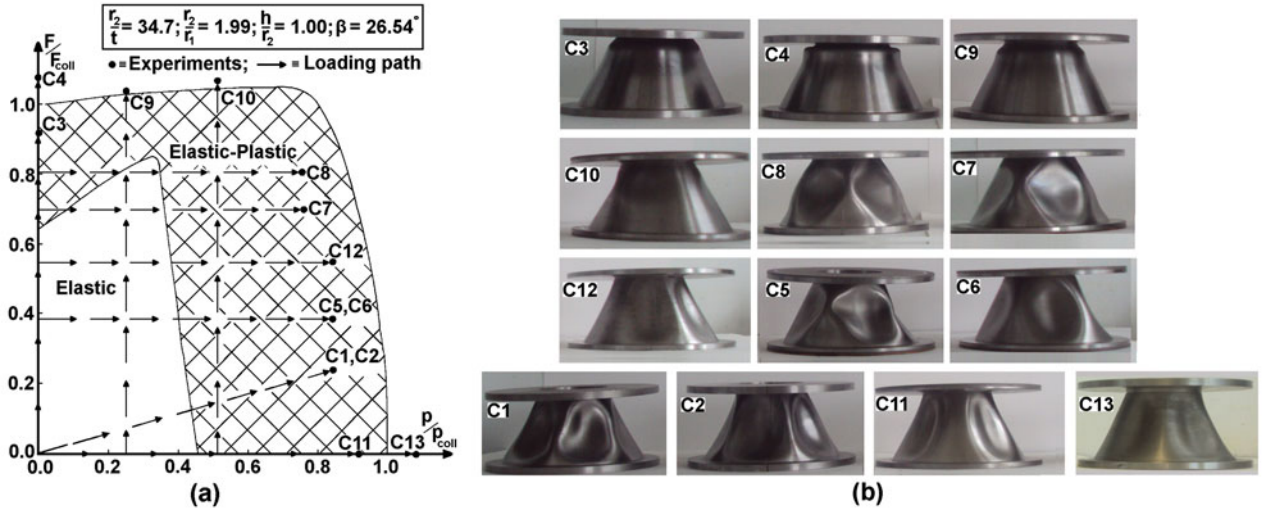

Figure 7. Illustration of loading paths for all tested cones (a) and the corresponding collapse shape after test (b). Note: In (a), the pressure axis is normalised by average experimental collapse pressure. The force axis is normalised by average experimental collapse force. (This figure is available in colour online.)

Table 3. Comparison of experimental and ASME predicted design load ($c \equiv$ constant force or pressure).

Model	Applied load	Experimental collapse load	ASME predicted design load
C1	Hydrostatic pressure (MPa)	8.0	5.36
C2	Hydrostatic pressure (MPa)	8.0	–
C3	Axial compression (kN)	238.98	114.17
C4	Axial compression (kN)	279.80	117.18
C5	F (kN)	100.0 (c)	89.16
	$p_{\text{coll}}^{\text{combined}}$(MPa)	7.90	5.33
C6	F (kN)	100.0 (c)	–
	$p_{\text{coll}}^{\text{combined}}$(MPa)	7.83	–
C7	F (kN)	180.0 (c)	120.63
	$p_{\text{coll}}^{\text{combined}}$(MPa)	7.17	4.52
C8	F (kN)	210.33 (c)	128.22
	$p_{\text{coll}}^{\text{combined}}$(MPa)	7.19	4.09
C9	$F_{\text{coll}}^{\text{combined}}$(kN)	268.96	128.29
	p (MPa)	2.414 (c)	1.58
C10	$F_{\text{coll}}^{\text{combined}}$(kN)	275.86	135.46
	p (MPa)	4.83 (c)	3.05
C12	F (kN)	143.0 (c)	107.62
	$p_{\text{coll}}^{\text{combined}}$(MPa)	8.07	4.89
C11	Lateral pressure (MPa)	8.56	4.70
C13	Lateral pressure (MPa)	10.36	-

the smallest of the values given by Equations (5) and (6),

$$\sigma_{\text{xc}} = \sigma_{\text{yp}}/\text{FS} \quad \text{for} \quad 2\rho_{\text{axial}}/t < 135 \tag{5a}$$

$$\sigma_{\text{xc}} = \sigma_{\text{yp}}/\text{FS} \quad \text{for} \quad 135 < 2\rho_{\text{axial}}/t < 600 \tag{5b}$$

$$\sigma_{\text{xc}} = \sigma_{\text{yp}}/\text{FS} \quad \text{for} \quad 2\,\rho_{\text{axial}}/t > 600 \tag{5c}$$

or

$$\sigma_{\text{xc}} = \sigma_{\text{xe}}/\text{FS} \tag{6}$$

where σ_{xe} is the elastic axial compressive membrane failure and σ_{yp} is the yield stress.

(3) Determine the allowable local hoop stress under external pressure only σ_{hc},

$$\sigma_{\text{hc}} = \sigma_{\text{yp}}/\text{FS} \ \text{ for } \ \sigma_{\text{he}}/\sigma_{\text{yp}} \geq 2.439 \tag{7a}$$

$$\sigma_{\text{hc}} = \sigma_{\text{yp}}/\text{FS} \ \text{ for } \ 0.552 < \sigma_{\text{he}}/\sigma_{\text{yp}} < 2.439 \tag{7b}$$

$$\sigma_{\text{hc}} = \sigma_{\text{yp}}/\text{FS} \ \text{ for } \ \sigma_{\text{he}}/\sigma_{\text{yp}} \leq 0.552 \tag{7c}$$

where σ_{he} is the elastic hoop compressive membrane failure.

(4) Determine the allowable stress in the longitudinal direction σ_{xac},

$$\sigma_{\text{xac}} = \left(\frac{1}{\sigma_{\text{xc}}^2} - \frac{C_1}{C_2 \sigma_{\text{xc}} \sigma_{\text{hc}}} + \frac{1}{C_2^2 \sigma_{\text{hc}}^2} \right)^{-0.5} \tag{8}$$

where

$$C_1 = \frac{(\sigma_{\text{xc}}\text{FS} + \sigma_{\text{hc}}\text{FS})}{\sigma_{\text{yp}}} - 1.0 \tag{9}$$

and

$$C_2 = \frac{f_x}{f_h} \tag{10}$$

$$f_h = \frac{2p(\rho_{\text{pressure}})}{2t} \tag{11}$$

$$f_x = \frac{F}{\text{Area}} + \frac{F_p}{\text{Area}} \tag{12}$$

where

$$\text{Area} = \pi(2\rho_{\text{axial}} - t)t \tag{13}$$

$$F_p = p\pi r_1^2 \tag{14}$$

(5) Determine the allowable hoop stress in the presence of axial compression σ_{hac}.

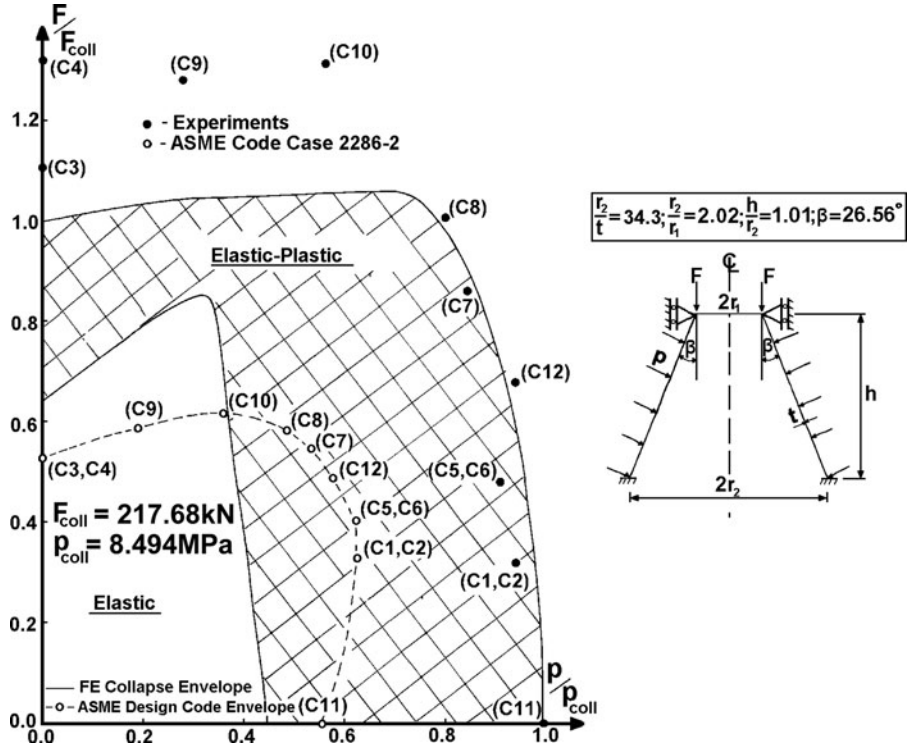

Figure 8. Domain of combined stability plot of ASME code case 2286-2 in comparison with numerically obtained combined stability plot for $r_2/t = 34.3$ using elastic perfectly plastic modelling.

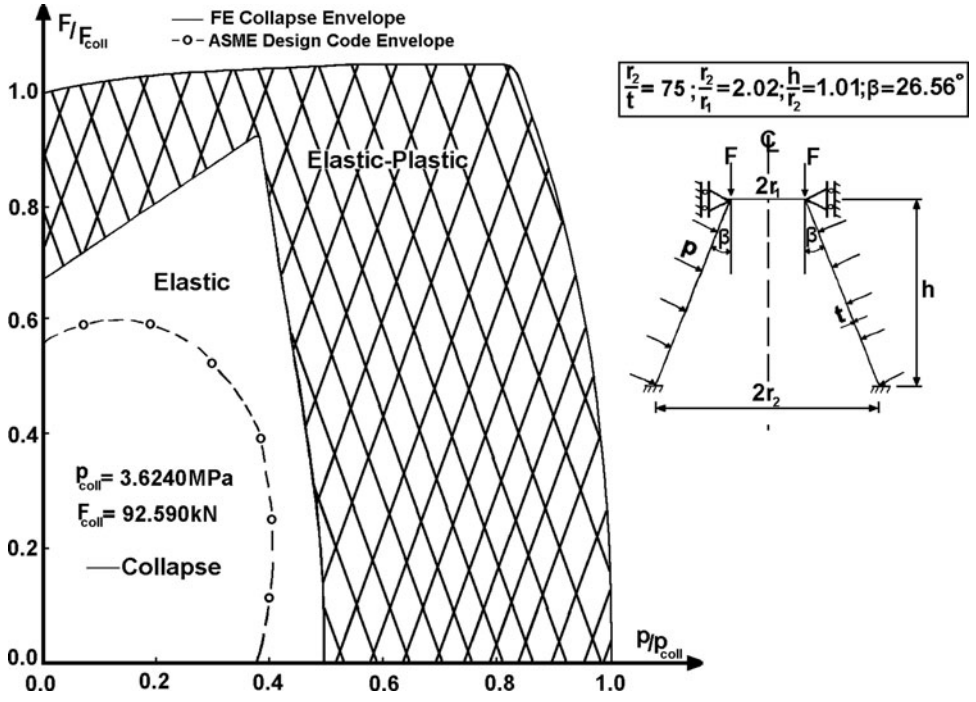

Figure 9. Domain of combined stability plot of ASME code case 2286-2 in comparison with numerically obtained combined stability plot for $r_2/t = 75$ using elastic perfectly plastic modelling.

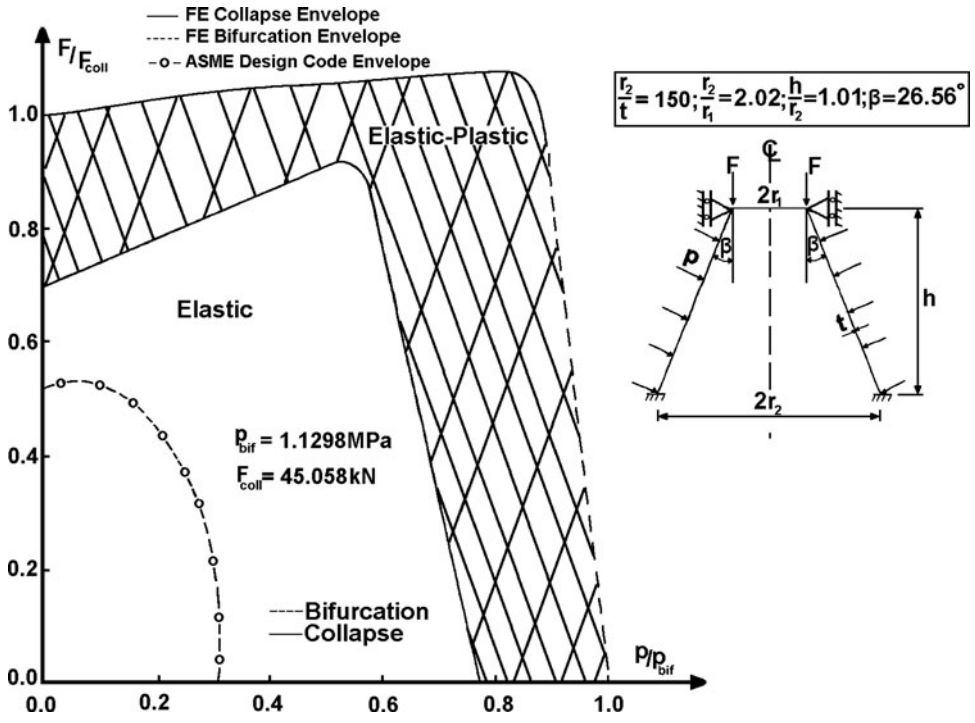

Figure 10. Domain of combined stability plot of ASME code case 2286-2 in comparison with numerically obtained combined stability plot for $r_2/t = 150$ using elastic perfectly plastic modelling.

$$\sigma_{\text{hac}} = \frac{\sigma_{\text{xac}}}{C_2} \tag{15}$$

With axial and hoop allowable stresses, one can obtain the design magnitude of axial force and external pressure subjected to combined loading as

$$F_{\text{des}} = \sigma_{\text{xac}} \times 2\pi t r_1 \cos\beta \tag{16}$$

$$p_{\text{des}} = 2\sigma_{\text{hac}} t / 2\rho_{\text{pressure}} \tag{17}$$

This design guideline was used to obtain the design magnitude for collapse pressure/axial compression for cones with radius-to-thickness ratio (r_2/t) of 34.3, 75, 150, and 250. The corresponding interactive curves are depicted in Figures 8, 9, 10, and 11, respectively.

Similar plot for cone with radius-to-thickness ratio (r_2/t) of 50 and cone's semi-vertex angle of 14° is reported in Blachut (2012). It can be observed that all the curves predicted by the design code follow similar trends. Also, it is noticed that decreasing the radius-to-thickness ratio of the cone leads to the design interactive plots becoming wider.

5. Comparison of experimental results and ASME design code predictions

In this paper, predictions given by ASME code case 2286-2 for failure load were compared with experimental results for cones C1, C3–C5, and C7–C12. The respective design magnitude of axial force and external pressure is given in column 4 of Table 3, and the corresponding interactive curve is depicted in Figure 8. It can be seen that all predicted results are on the safe side of the experimental results.

Also, it can be seen from Figure 8 that the ASME design code envelope is on the safe side of the first yield envelope in the 'force dominant region', but on the unsafe side of the first yield envelope in the 'pressure dominant region'. For use in design, especially for cones that fail within the elastic–plastic range, this is quite dangerous as it induces a permanent deformation on the cone, thereby reducing the cone's load-carrying capacity. Hence, it is important to establish the range of applicability of this design codes.

From Figures 9 to 11, it can be observed that for cones with radius-to-thickness ratio $r_2/t \geq 75$, the ASME design code envelope is on the safe side of the first yield envelope. Therefore, for cones with radius-to-thickness ratio $r_2/t \geq 75$, the ASME design code is adequate and sufficient in predicting the combined stability envelope, whilst for $r_2/t < 75$, this design code is unsafe.

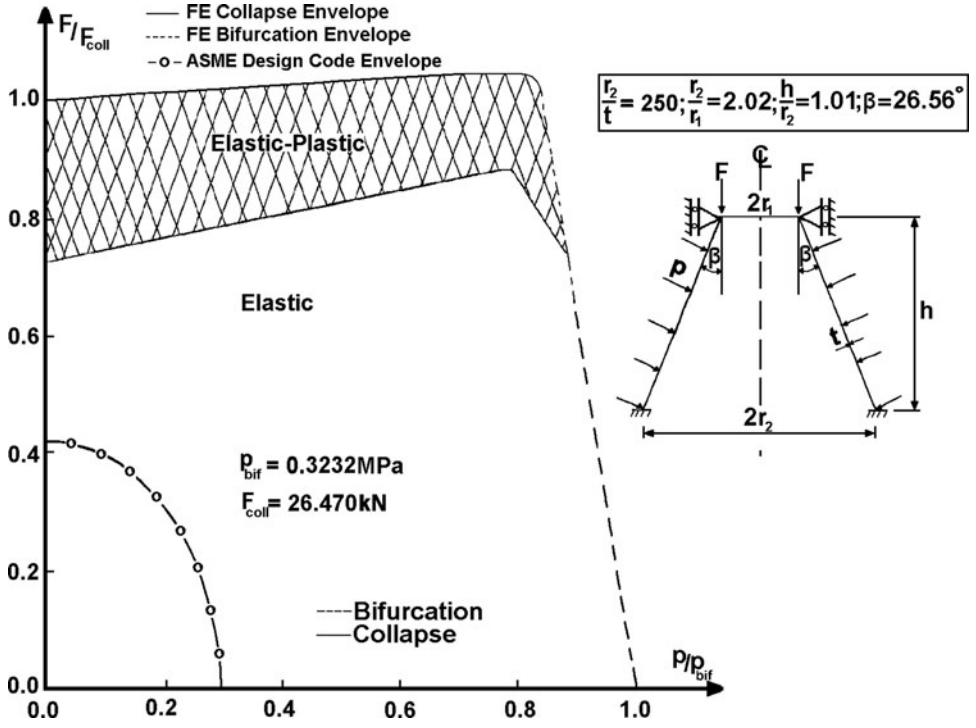

Figure 11. Domain of combined stability plot of ASME code case 2286-2 in comparison with numerically obtained combined stability plot for $r_2/t = 250$ using elastic perfectly plastic modelling.

6. Conclusion

It has been found that for thick cones under repeated loading subjected to combined axial compression and external pressure acting simultaneously, the ASME code case 2286-2 design code envelope is on the safe side of the first yield envelope in the 'force dominant region', but on the unsafe side of the first yield envelope in the 'pressure dominant region' for cones with radius-to-thickness ratio $r_2/t < 75$. Whereas, for cones with radius-to-thickness ratio $r_2/t \geq 75$, the ASME interactive design prediction is safe. Therefore, this study concludes that the ASME code case 2286-2 design procedure for cones under combined loads (i.e., axial compression and external pressure) is only sufficient in predicting the interactive plots for cones with $r_2/t \geq 75$ and not appropriate for cones with $r_2/t < 75$.

Also, it has been shown that the concept of equivalent cylinder approach for a thick master cone with radius-to-thickness ratio $r_2/t = 34.3$ is not conservative, as the combined stability plot of the equivalent cylinder overestimates the load-carrying capacity of its conical counterpart. This makes the approach unsafe for design purposes. This study offers only a limited insight into the equivalent approach for thick master cone. Therefore, further work using different radius-to-thickness would be desirable.

Nomenclature

E	Young's modulus
F	Applied axial compressive load
FS	Stress reduction factor
F_{des}	Design axial compressive buckling load
F_{p}	Axial compression load resulting from applied external pressure
K	Boundary conditions at the ends
L_u	Length of unsupported member
f_h	Hoop compressive membrane stress resulting from applied external pressure p
p	Applied external pressure
p_{des}	Design external pressure load
r	Radius of gyration
r_1	Radius at the small end of the cone
t	Shell wall thickness
β	Cone semi-vertex angle
λ_c	Slenderness factor
σ_{hac}	Allowable hoop compressive membrane stress in the presence of axial compression
σ_{hc}	Local hoop stress under pressure only
σ_{he}	Elastic hoop compressive membrane failure
σ_{xac}	Allowable axial compressive membrane stress in the presence of hoop compression
σ_{xc}	Local compressive membrane stress due to axial compression
σ_{xe}	Elastic axial compressive membrane failure
σ_{yp}	Yield stress
ρ_{axial}	Equivalent cylinder radius under axial compression
ρ_{pressure}	Equivalent cylinder radius under external pressure

References

[ASME] American Society of Mechanical Engineers. 2008. Code Case 2286-2, Alternative rules for determining allowable external pressure and compressive stresses for cylinders, cones, sphere and formed heads, Section VII, Divisions 1 and 2. Cases of the ASME boiler and pressure vessel code. New York (NY): American Society of Mechanical Engineers. p. 1–13.

Barkey ME, Turgeon MC, Varun Nare T. 2008. Buckling of stiffened thin-walled truncated cones subjected to external pressure. Exp Mech. 48:281–291.

Blachut J. 2010. Elastic-plastic buckling of cones under combined loading. In: Topping BHV, Adam JM, Pallares FJ, Bru R, Romero ML, editors. Proceeding of the Tenth International Conference on Computational Structures Technology. Stirlingshire (UK): Civil-Comp Press. Paper 155. p. 1–12.

Blachut J. 2011. On elastic-plastic buckling of cones. Thin Wall Struct. 49(1):45–52.

Blachut J. 2012. Interactive plastic buckling of cones subjected to axial compression and external pressure. Ocean Eng. 48:10–16.

Blachut J, Ifayefunmi O. 2012. Buckling of unstiffened steel cones subjected to axial compression and external pressure. J Offshore Mech Arct Eng, Trans. ASME. 134(3):031603-1–031603-9.

DIN 18 800. 1990. Structural steelwork: analysis of safety against buckling of shells. Berlin (Germany): Deutsche Norm.

DnV CN 30.1. 1992. Buckling strength analysis. Oslo (Norway): Det Norske Veritas.

ECCS TWG 8.4. 2008. Buckling of steel shells: European design recommendations. 5th ed. Brussels (Belgium): European Convention for Constructional Steelwork.

Hibbitt, Karlsson, Sorensen. 2006. ABAQUS - theory and standard user's manual. Version 6.4. Providence (RI): Hibbitt, Karlsson & Sorensen, Inc.

Ifayefunmi O. 2011. Combined stability of conical shells [PhD Thesis]. Liverpool (UK): University of Liverpool.

Ifayefunmi O, Blachut J. 2012. Combined stability of unstiffened cones – theory, experiments and design codes. Int J Pres Ves Pip. 93–94:57–68.

Lackman L, Penzien J. 1960. Buckling of circular cones under axial compression. J Appl Mech. 27(3):458–460.

Samuelson LA, Eggwertz S. 1992. Shell stability handout. Essex (UK): Elsevier Science Publishers Ltd. p. 100–106.

Schmidt H, Krysik R. 1994. Static strength of transition cones in tubular members under axial compression and internal pressure. In Balkema AA, editor. Tubular structures. Proceedings of the Sixth International Symposium; 1994 Dec 14–16; Melbourne, Australia. p. 163–168.

Seide P. 1956. Axisymmetrical buckling of circular cones under axial compression. J Appl Mech. 23:625–628.

Seide P. 1959. On the buckling of truncated conical shells under uniform hydrostatic pressure. Symposium on the theory of thin elastic shells. Proceedings of the International Union of Theoretical and Applied Mechanics; Delft, Holland. p. 363–388.

Singer J. 1962. Buckling of orthotropic and stiffened conical shells. Washington (DC): NASA TN-D-1510. p. 463–475.

Singer J. 1963. Correlation of the critical pressure of conical shells with that of equivalent cylindrical shells. AIAA J. 1(11):2675–2676.

Singer J. 1965. On the buckling of unstiffened orthotropic and stiffened conical shells. Proceedings of Seventhth Congress of International Aeronautique; 14–16 June, Paris. p. 1–22.

Singer J. 1966. Buckling of clamped conical shells under external pressure. AIAA J. 4(2):328–337.

Singer J, Arbocz J, Weller T. 2002. Buckling experiments: experimental methods in buckling of thin-walled structures. Vol. 2, New York (NY): Wiley. p. 722–723.

Singer J, Eckstein A. 1963. Recent experimental studies of buckling of conical shells under torsion and external pressure. Proceedings of the Fifth Israel Conference on Aviation and Astronautics; Jerusalem: Academic Press. p. 135–146.

Tani J. 1971. Influence of prebuckling deformations on the buckling of truncated conical shells under axial compression. Jpn Soc Aeronaut Space Sci. 232–245.

Weingarten VI, Morgan EJ, Seide P. 1965. Elastic stability of thin-walled cylindrical and conical shells under axial compression. AIAA J. 3(3):500–505.

Yeh KY, Sun BH, Rimrott FPJ. 1995. Buckling of imperfect sandwich cones under axial compression – Equivalent cylinder approach, Part II. Tech Mech. 15(1):1–12.